Soft Matter

Cite this: *Soft Matter*, 2012, **8**, 6950

www.rsc.org/softmatter

PAPER

Characterization of dynamics and internal structure of a mixed-surfactant wormlike micellar system using NMR and rheometry

Suliman Barhoum,*[a] Rolando Castillo[b] and Anand Yethiraj[a]

Received 31st January 2012, Accepted 26th April 2012
DOI: 10.1039/c2sm25237f

We use complementary experiments—proton NMR diffusometry and relaxometry, deuterium NMR lineshapes, and rheometry—to construct a comprehensive picture of the microscopic structure of a mixed-surfactant wormlike micellar system composed of a zwitterionic surfactant and an anionic surfactant in brine. In this system, at some surfactant concentrations, the time for micellar breaking and recombination τ_b is not small compared with the micellar reptation time τ_R, weakening the condition to obtain a stress relaxation function with just one relaxation time at long times. From NMR relaxometry, we determine the overlap concentration. Deuterium NMR spectral lineshapes indicate the presence of a wide angular distribution in the orientational order. NMR diffusometry and rheology probe different timescales and yield complementary information indicating polymer-like behaviour at the corresponding lengthscales. *Via* NMR, surfactant diffusion coefficients are seen to decrease with increasing diffusion time, consistent with restricted diffusion within a reptating micelle. At the same time, comparison of measurements with protonated and deuterated surfactants strongly suggests that the measured short and long time diffusion coefficients correspond to intra-micellar and micellar diffusion, respectively. Fitting the diffusion results to a simple model, the average end-to-end micellar distance is estimated to be in the 1 μm range and only weakly dependent on concentration. The water diffusion measurements, on the other hand, imply a high degree of water structuring at the micellar surface. We also find that the wormlike micelles obeyed simple polymer-like scaling behaviors, with a crossover from Zimm-like (diffusion) to Rouse-like (rheology) exponents.

Introduction

Amphiphilic molecules in aqueous solution form aggregates with different structures such as bilayers, vesicles, and spherical, cylindrical or wormlike micelles, depending on molecular geometry as well as on the net charge and surfactant concentration.[1] Wormlike micelles are interesting, due to the fact that they are elongated objects like polymers (which have interesting dynamics and hydrodynamic effects[2–5]); however, they continuously break and recombine.[6–10] This has technological applications (from heat-transfer fluids to oil-field applications to drain-openers[9]) because, unlike normal polymers, they can reform after breaking and can thus survive repeated shear.[6]

Much work has been carried out on the study of wormlike micelles *via* theory[8,11–13] and computer simulation,[14,15] and there have been several reviews on the subject.[6,7,10,15,16] Experimentally, wormlike micellar systems can be composed of cationic, anionic, zwitterionic or non-ionic surfactants.[6,8,17–20] Mixtures of cationic and anionic surfactants,[20] zwitterionic dimeric surfactant solutions[21] and cationic surfactant solutions[20,22] have also been investigated. A common surfactant in wormlike micelle literature is cetyl trimethylammonium bromide (CTAB)[23–27] which forms cylindrical wormlike surfactant micelles; systems forming reverse micelles have also been reported.[28,29]

Small-angle neutron scattering and dynamic light scattering studies have reported on isotropic to nematic phase transitions,[23] transitions from vesicles to wormlike micelles,[30] the concentration dependence of the hydrodynamic correlation length,[31] and the effect of adding salt on micellar growth.[32] Scattering measurements have also characterized important lengths of the micellar network[33] and have been used to investigate local structure and flexibility.[34,35] A combination of rheology and small angle neutron scattering (Rheo–SANS) has also been used to study concentration dependencies of shear thinning and alignment in a block copolymer wormlike micellar system.[36]

Pulsed-field-gradient nuclear magnetic resonance was used to identify sub-diffusive behavior in a wormlike reverse micelle system.[37] This technique has been employed in other (polymer and protein) soft matter systems[38,39] to provide information that is complementary to scattering methods, and is especially useful when the system contains large and/or multi-component aggregates. This is because spectral separation of different chemical

[a]*Department of Physics and Physical Oceanography, Memorial University, St. John's, NL, Canada. E-mail: sulimanb@mun.ca; Ayethiraj@mun.ca*
[b]*Instituto de Fisica, Universidad Nacional Autónoma de México, P. O. Box 20-364, Mexico D.F. 01000, Mexico. E-mail: rolandoc@fisica.unam.mx*

components is easy in NMR, challenging in scattering, and practically impossible in rheology.

Recently, a multi-component system consisting of a mixture of two similar-sized surfactants, one zwitterionic (*N*-tetradecyl-*N*,*N*-dimethyl-3-ammonio-1-propanesulfonate or TDPS) and the other anionic (sodium dodecyl sulfate or SDS), in brine[33,40,41] has been studied by rheology and scattering techniques. The TDPS–SDS system was studied at a range of TDPS concentrations C_z, spanning both dilute and semidilute regimes at different surfactant ratios R = [SDS]/[TDPS] and different temperatures.[33,40,41] The average micelle contour length was found to be in the micron range and (for $R = 0.55$) to increase with C_z when the wormlike micelles are totally screened by salt addition, while the "mesh size" reflecting intermicellar correlations is in the 50–100 nm regime and insensitive to changes in C_z, surfactant concentration ratio or temperature.[33] An interesting feature of this system is that while $R = 0.55$ mixtures could be fitted to Maxwellian viscoelastic behavior with a single relaxation time for the stress relaxation modulus G(t) at long times,[41] those for $R = 0.43$–0.45 show deviations from the Maxwellian model.[41] Two timescales are relevant in wormlike micellar systems. τ_b refers to the breaking/recombination timescale, while τ_R is the reptation timescale. If the micellar chain breaks and recombines many times during the reptation process (*i.e.* $\tau_R \gg \tau_b$), the tube-like contour segments exhibit a single relaxation rate.[8]

In our previous work,[38] we have shown that mixed-species (polymer–surfactant) aggregates are easier to study than single-species (surfactant) aggregates because the dynamics of each species can be independently and simultaneously measured *via* complementary NMR experiments. This allows models of aggregate structure to be sufficiently constrained. In this work, using the TDPS–SDS system (with $R = 0.45$), we obtain in unprecedented detail both the structure and dynamics in a system where the linear rheology is not dominated by a single relaxation time at low frequencies.

In this work, we use NMR diffusometry and relaxation measurements, as well as deuterium NMR, to explore the dynamics and the structure of the micellar aggregates. Relaxation in NMR usually refers to two processes by which nuclear magnetization prepared in a non-equilibrium state returns to the equilibrium distribution. Different physical processes are responsible for the relaxation of the components of the nuclear spin magnetization vector M, parallel and perpendicular to the external magnetic field, B_0 (which is conventionally oriented along the z-axis). These two principal relaxation processes are termed T_1 and T_2 relaxation, respectively. The longitudinal T_1 and transverse T_2 relaxation times can be measured directly using NMR, and can be used to report on changes in the local environment.[42]

In the NMR diffusion experiment, the sample experiences both an external uniform magnetic field from the magnet and a non-uniform spatially well-defined magnetic field (*i.e.* pulsed field gradient). Therefore, the molecular diffusion is measured from the signal attenuation that arises from the dephasing of nuclear spin coherence.[43,44] Deuterium NMR, on the other hand, is an effective probe of the orientational order of the deuterated hydrocarbon chains.[45] Thus, we are able to obtain independent dynamical information on all components in a 3-component system *via* spectral separation (*via* a difference in either chemical shift or spin label) of diffusion coefficients.

Utilizing these complementary NMR techniques on the TDPS–SDS system (with $R = 0.45$), in tandem with rheology, we obtain in unprecedented detail both the structure and dynamics in the case where the linear rheology of the system is not dominated by a single relaxation time at low frequencies.

Experimental

Materials

N-Tetradecyl-*N*,*N*-dimethyl-3-ammonio-1-propanesulfonate (TDPS, M_w = 363.6, purity >99%), sodium dodecyl sulfate (SDS, M_w = 288.38, purity >99%), and SDS-d25 (M_w = 313.53, 98 atom% D) were purchased from Sigma-Aldrich Canada and were used as received. We prepared stock solutions of TDPS–SDS(0.5 M)–D_2O as well as TDPS–SDS-d25–NaCl(0.5 M)–H_2O at C_z = 50 mM, as well as the brines NaCl(0.5 M)–D_2O and NaCl(0.5 M)–H_2O. Samples with TDPS concentration and protonated/deuterated SDS below 50 mM (in the semidilute regime) were prepared by diluting with brine made with D_2O/H_2O respectively. The sample in the concentrated regime C_z = 140 mM was prepared separately. The surfactant ratio in all samples was R = [SDS]/[TDPS] = 0.45. Deuterium oxide D_2O (for all protonated SDS samples) and deuterium-depleted H_2O (for deuterated SDS samples) were purchased from Cambridge Isotope Laboratories. While surfactant mixtures were prepared by addition of constituents by mass, the volume fraction is the relevant quantity when considering hydrodynamic corrections. We estimate a volume fraction Φ using

$$\Phi = \frac{V_{TDPS} + V_{SDS}}{V_{TDPS} + V_{SDS} + V_{NaCl(0.5M)-H_2O}} \quad (1)$$

where $V_\alpha = m_\alpha/\rho_\alpha$, V_α, m_α and ρ_α are the volume, mass and density of the α component in solution, and α indicates TDPS, SDS or NaCl(0.5 M)–H_2O. Note that this is an estimate of volume fraction due to the assumption of volume additivity. Because of the densities ($\rho_{SDS} = \rho_{TSDS} \approx 1$ g cm^{-3}, and $\rho_{NaCl(0.5\ M)-H_2O} \approx 1.02$ g cm^{-3}), our estimated volume fraction is essentially equivalent to the mass fraction.

NMR spectra were collected on a Bruker Avance II spectrometer with a ^{1}H resonance frequency of 600.33 MHz and a ^{2}H resonance frequency of 92.15 MHz. We can easily separate the water peak at 4.7 ppm and the surfactant peaks spectrally in the NMR spectrum. However, due to the broad (super-Lorentzian) lineshapes, we are unable to spectrally separate the TDPS and SDS peaks (0–4 ppm). Thus, we prepared some samples with deuterated SDS. We were then able to compare the surfactant dynamics of TDPS (proton NMR with deuterated SDS yields only the TDPS peaks) with the surfactant dynamics of TDPS–SDS peaks in protonated SDS samples.

Relaxation measurements were performed using a Micro-5 imaging (3-axis gradient) probe. The inversion recovery technique was used to measure T_1: sixteen time delays were used, and the integrated intensities in the spectrum were fitted to the equation: $I(t) = I_0(1 - 2\exp(-t/T_1))$.[42] A $(\pi/2)_x - t/2 - (\pi)_x - t/2$-acquire spin echo experiment was used to measure T_2: 16 values, at delay time t, of the integrated intensity were taken to measure T_2 and were fitted to the equation: $I(t) = I_0 \exp(-t/T_2)$.[42]

Three-axis self-diffusion measurements were carried out in a Micro-5 imaging (3-axis gradient) probe with a maximum gradient strength of 200 G cm^{-1} or a Diff30 diffusion probe with a maximum field gradient 1800 G cm^{-1}, employing a pulsed-field gradient stimulated-echo sequence[44] with (almost square) trapezoidal gradient pulses, with the rise time of the trapezoid (the gradient ramp time) being 100 μs, *i.e.* much smaller than the diffusion time Δ or the total duration δ of the field gradient pulse. In our experiments, δ = 2 ms, and the gradient g was varied in steps from 0% to ≈100%. For deuterated SDS samples, ^{2}H NMR spectra were collected using a $(\pi/2)_x - t - (\pi/2)_y - t$-acquire quadrupole echo experiment using 256 scans, and with t = 10 μs.

Spectrally resolved molecular diffusion coefficients along the field direction (D_z) and perpendicular to the field direction (D_x and D_y) are obtained from the attenuation of the signal according to the equation:[43]

$$D = \frac{-1}{k}\ln\left(\frac{S(k)}{S(0)}\right) \quad (2)$$

where S(k) is the integrated intensity of the signal in the presence of the field gradient, while S(0) is the intensity of the signal in the absence of the field gradient, and $k = (\gamma\delta g)^2(\Delta - \delta/3)$ is a generalized gradient strength parameter. The diffusion time Δ is the duration of the pulse sequence in which molecular diffusion has an effect on the signal attenuation. The signal attenuation as a function of k associated with TDPS–SDS peaks is a single exponential (Fig. 1) over the whole range of TDPS concentrations. When there is free bulk diffusion, the diffusion coefficient does not depend on the diffusion time Δ.

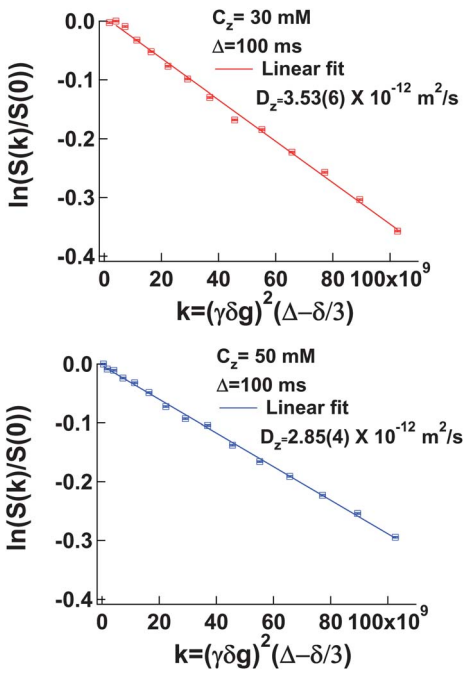

Fig. 1 Natural logarithm of the signal attenuation *versus* the gradient strength parameter $k = (\gamma\delta g)^2(\Delta - \delta/3)$ with Δ = 100 ms for (top) TDPS(30 mM)–SDS(13.5 mM)–NaCl(0.5 M)–D_2O and (bottom) TDPS(50 mM)–SDS(22.5 mM)–NaCl(0.5 M)–D_2O samples at T = 298 K. The spectral region 0–4 ppm is used to measure the surfactant signal attenuation.

Rheometry

Rheological measurements were carried out on an Anton Paar Physica MCR 301 rheometer. All the rheometric measurements were done at T = 298 K using the cone–plate geometry of 50 mm diameter and 0.5° cone angle. The stress relaxation experiments were performed with an applied shear strain $\gamma = 0.5$. The flow curve experiments were carried out with shear strain rate $\dot{\gamma}$ varying from 0.001 to 150 s^{-1} to extract the zero-shear strain viscosity η. In addition, the oscillatory shear experiments were performed with an angular frequency ω varied in log-ramp from 50 rad s^{-1} to 0.01 rad s^{-1}.

Results and discussion

NMR relaxation and the overlap concentration

Longitudinal T_1 and transverse T_2 relaxation measurements were carried out for TDPS–SDS–NaCl(0.5 M)–D_2O samples at different TDPS concentrations, C_z. The proton longitudinal relaxation time T_1 (Fig. 2) can be fit to a mono-exponential decay, with a significant decrease as one crosses the overlap concentration (reported to be at 7 mM by Lopez-Diaz *et al.*[40]). The change in T_1 indicates a change in the local environment for the surfactant molecules, which corresponds well with the wormlike micelle overlap concentration. Based on the exponential fit, we extract a characteristic concentration of $C^{threshold} = 4.5 \pm 0.4$ mM (*i.e.* $C^{threshold} \approx C^*$). The T_2 relaxation time (not shown) shows no appreciable change as a function of TDPS concentration C_z.

Deuterium NMR and orientational structure

Measurements with deuterated SDS provide good opportunities to look at the orientational structure of the SDS (using deuterium NMR), and to separate the dynamics of the TDPS (using proton diffusometry). We also use these samples to measure the variation of the water diffusion coefficient with surfactant concentration.

Fig. 3a shows ^{2}H NMR spectra for C_z = 46 mM as a function of temperature. The appearance of a single broad peak in the deuterium NMR spectrum implies a structure that is intermediate between an isotropic liquid and an oriented liquid. It is likely an indication of the presence of a liquid crystal like mesophase with a wide orientational angular distribution. As we will describe below, this is consistent with the interpretation of

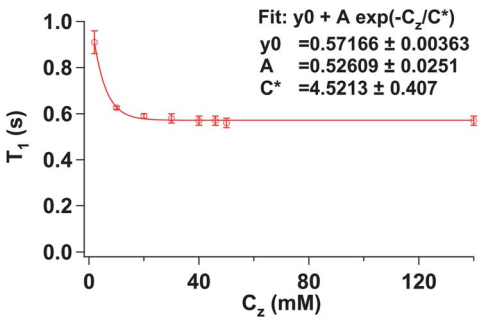

Fig. 2 Proton longitudinal relaxation time T_1 *versus* TDPS concentration C_z for TDPS–SDS–NaCl(0.5 M)–D_2O samples at T = 298 K.

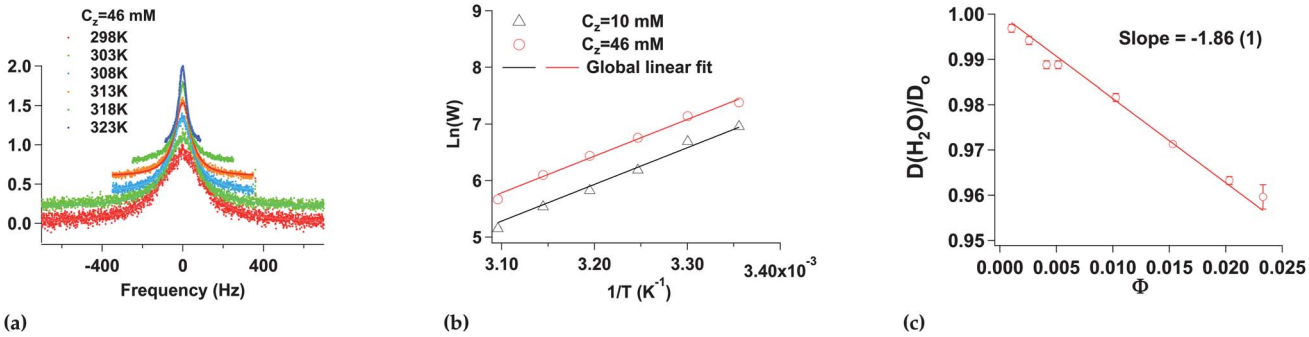

Fig. 3 (a) The deuterium NMR lineshape fits well to a Lorentzian function. The peak width W for $C_z = 46$ mM decreases with increasing temperature in the range 298 K to 323 K. (b) The peak width W exhibits an Arrhenius temperature dependence: results for $C_z = 10$ mM and 46 mM can both be fitted with a single activation energy. (c) The relative H_2O diffusion coefficient *versus* total surfactant volume fraction Φ in TDPS–SDS–d25–NaCl(0.5 M)–H_2O samples at $T = 298$ K.

Fig. 4a, where we see only a small anisotropy in the measured diffusion coefficient. This averages out the first-order quadrupole coupling.[46] We may fit the deuterium NMR lineshape to the absorption Lorentzian function

$$S(\omega) = \frac{(W/2)}{(W/2)^2 + (\omega - \omega^0)^2} \quad (3)$$

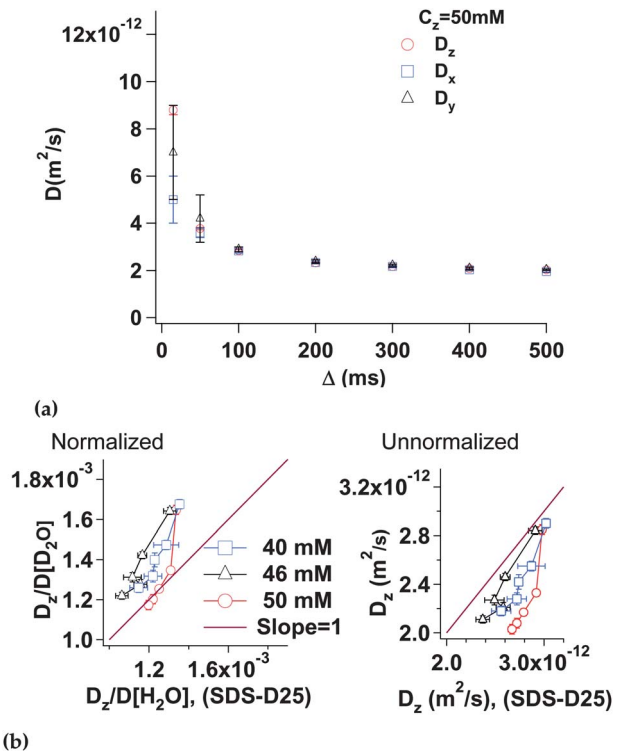

Fig. 4 (a) TDPS–SDS self-diffusion coefficient (D_x,D_y,D_z) *versus* diffusion time Δ. $C_z = 50$ mM. (b) Relative z-self diffusion coefficient $\frac{D_z}{D[D_2O]}$ of TDPS–SDS–NaCl(0.5 M)–D_2O *versus* $\frac{D_z}{D[H_2O]}$ of TDPS–SDS-d25–NaCl(0.5 M)–H_2O (left). If the values were equal they would be on the 45 degree line and D_z for non-deuterated SDS samples *versus* that for deuterated SDS samples (right). $C_z = 40$ mM, 46 mM and 50 mM at $T = 298$ K, with diffusion times ranging from $\Delta = 100$ to 500 ms.

where ω and ω^0 are the frequency coordinates and the Larmor frequency of the deuterium (spin-1) nuclei, respectively. W is the deuterium peak width at half maximum of the absorption peak.

For deuterated SDS samples (TDPS–SDS-d25–NaCl(0.5 M)–H_2O) at two TDPS concentrations ($C_z = 10$ and 46 mM), we can extract the deuterium peak width at half maximum (W) of the absorption peak as a function of temperature between 298 K and 323 K. The width of the SDS peak at 298 K is ~200 Hz (about a factor of 10 larger than an HDO peak when deuterium-depleted water is not used). In general, a single-Lorentzian peak could result either from exchange mediated by a free surfactant monomer in solution or by the surfactant seeing a continuous change in orientational order while diffusing inside a curvilinear micelle. Given the peak width, diffusion inside a micelle with a continuously changing orientation seems to dominate the signal represented by the broad isotropic peak. Using a surfactant diffusion coefficient $D_s = 13 \times 10^{-12}$ m^2 s^{-1}, and the experimental timescale of 10 μs yields a lengthscale of $\ell = \sqrt{6\tau D_s} \sim 28$ nm. This is roughly consistent with the values (~35 nm) reported for the persistence length in this system.[33] A similar broadening of a broad isotropic peak with decreasing temperatures has been seen in so-called "stiff gel" smectics in the presence of a high density of quenched random disorder, which has been interpreted, not as a true isotropic phase, but as a smectic phase with a wide and smooth angular distribution of the orientational order.[45] This peak width shows an Arrhenius temperature dependence. By globally fitting both data sets in Fig. 3b to one exponential function $W = A\exp(E_a/k_BT)$, we estimate the activation energy to be $E_a \approx 21.8(1)k_BT \approx 54$ kJ mole^{-1}; this represents the barrier for surfactant diffusion in these wormlike micelles.

Water diffusion in aqueous surfactant solutions has been shown to be a weighted average of two kinds of water, bulk water and surface associated water.[47] The water molecule is polar, and it associates with a surface of charged molecules or charged aggregates. It has been shown to be a reasonable approximation to assume that the surface-associated water is essentially stationary in comparison to the bulk water.[38,47] Thus, water diffusion coefficient obtained as a function of surfactant packing fraction report directly on the fraction of surface associated water. Fig. 3c shows the variation of the relative self-diffusion

coefficient of H_2O molecules in TDPS–SDS-d25–NaCl(0.5 M)–H_2O over the range of total surfactant volume fraction Φ from 0.001 to 0.023.

The H_2O diffusion coefficient values are scaled to the bulk diffusion coefficient (*i.e.* $D_o = 2.23 \times 10^{-9}$ m^2 s^{-1}) of a H_2O molecule in 0.5 M brine, which we also measured. The decrease in H_2O diffusion coefficient with increasing surfactant volume fraction arises from H_2O molecules associating with the surface of charged cylindrical TDPS–SDS micelles in the aqueous solution. An admittedly oversimplified picture is one where a water molecule diffuses freely until it meets a micelle, at which point it either sticks or bounces, with the molecules that stick assumed to be static (this is valid since the surfactant diffusion coefficient is 3 orders of magnitude smaller than that of water). From simple geometry for a cylindrical micelle, we related the observed diffusion coefficient to the thickness of the water layer, h, and the diameter of the bare cylindrical micelle, d:

$$\frac{D}{D_o} \approx 1 - \left(1 + 4\left(h/d + (h/d)^2\right)\right)\Phi \quad (4)$$

A single H_2O monolayer has thickness 0.3 nm. Fitting the observed diffusion coefficient in Fig. 3c, we find that $h/d = 0.182 \pm 0.004$. Allowing for the surface-associated water to diffuse like the surfactant diffusion modifies this result slightly to $h/d = 0.186 \pm 0.004$. Given a micellar diameter of $d \approx 6$ nm,[40] this implies a water layer thickness of $\approx$3 to 4 monolayers.

Three-axis diffusometry and micelle structure

The observed self-diffusion coefficient (Fig. 4a) measured along the z, x, and y axes displays a very similar behaviour, and thus exhibits insignificant ordering effects in the $\approx$14 T magnetic field. D_z, D_x and D_y all decrease as a function of diffusion time Δ. If what we measure is only the self-diffusion of the wormlike micelle, then we would not expect D to show a dependence on Δ. For $\Delta \geq 15$ ms, the wormlike micelle is already in the long-time limit due to the fact that RMS displacement over the millisecond timescale is much larger than the average mesh size of the TDPS–SDS–NaCl(0.5 M) micellar solution $\xi \approx 75$ nm.[33] The observed decrease of D with Δ suggests strongly that the observed diffusion coefficient is a combination of micellar self-diffusion and surfactant self-diffusion inside the micelle.

This is confirmed by comparing surfactant diffusion coefficients for systems with non-deuterated and fully deuterated SDS. This is akin to contrast matching experiments in neutron scattering. The surfactant self diffusion coefficient D_z was measured for TDPS–SDS-d25–NaCl(0.5 M)–H_2O samples with deuterated SDS at 3 TDPS concentrations (40 mM, 46 mM, and 50 mM). Here, we measure the TDPS self-diffusion coefficient, whereas in the protonated samples one measures an average value of TDPS and SDS diffusion coefficients. If the two values are equal, they will lie on the 45 degree line. The values obtained for the relative diffusion coefficients in Fig. 4b (left) are only close to being equal at the smallest values (corresponding to the largest Δ (500 ms)), where $D[H_2O] = 2.23 \times 10^{-9}$ m^2 s^{-1} and $D[D_2O] = 1.73 \times 10^{-9}$ m^2 s^{-1} are the diffusion of H_2O and D_2O, respectively, in 0.5 M brine. This is consistent with the notion that the micellar diffusion coefficient should depend only on the micelle size and the solvent viscosity. Therefore, assuming a Stokes–Einstein-like relationship for the micelle in the solvent $D \propto 1/\eta$, the diffusion coefficient relative to the solvent diffusion coefficient should be the same for both systems.

Fig. 4b (right) on the other hand shows the bare self diffusion coefficients D_z. Here we see that the values for the deuterated and non-deuterated samples are closest for small Δ (100 ms) (*i.e.* for large D_z). This is consistent with surfactant diffusion within the micelle—these values should indeed be insensitive to solvent viscosity.

Three-axis diffusion measurements thus show that there is very insignificant anistropy in the wormlike micelle conformations in the presence of a large magnetic field. Moreover, comparison of the measurements in the deuterated and non-deuterated surfactant show a clear trend: micellar diffusion is dominant for large Δ, while intramicellar diffusion is dominant for small Δ.

Micellar and intramicellar diffusion

From the observed values of anisotropic self-diffusion coefficients (Fig. 4a) at different diffusion times Δ, the mean-square displacement (MSD) values ($MSD_i = 2D_i\Delta$, i = x,y,z) are obtained (Fig. 5a). The dependence is clearly very linear; however the straight line does not pass through the origin. Therefore, the diffusion is neither lateral diffusion[48] nor is it single-file diffusion[49] for which the MSD should scale as the square root of the diffusion time. The slope in Fig. 5a represents a reasonable estimate for the micellar diffusion (Fig. 5b) at different TDPS concentrations C_z. The non-zero intercept, on the other hand, is an indication of faster intra-micellar surfactant diffusion at shorter times.

Fig. 5b shows the variation of the anisotropic micelle diffusion coefficients $(D_m)_x$, $(D_m)_y$ and $(D_m)_z$ of the micelle as a function of TDPS concentration in the semidilute regime (*i.e.* 10 mM $\leq C_z \leq$ 50 mM) for $(D_m)_x$, $(D_m)_y$ and in the 10 mM $\leq C_z \leq$ 140 mM regime for $(D_m)_z$ of TDPS–SDS–NaCl(0.5 M)–D_2O. The anisotropic diffusion curves D_z and D_y are offset along the y-axis. The anisotropic self-diffusion coefficients exhibit a power law decrease with respect to C_z.

We globally fit the three datasets in Fig. 5b in the semidilute regime to a single power law ("Global fit" in graph). Our experiments yield a power law $D = D_{Zimm}(C_z/C^*)^{-d}$ with the exponent $d = 0.58 \pm 0.03$. The Zimm model for polymer dynamics in a good solvent considers the hydrodynamic interactions between the monomers on the polymer chain and between the monomers and the solvent molecules in the pervaded volume. It would predict an exponent $d = (1 - \nu)/(3\nu - 1) = 0.54$ (using $\nu = 0.588$ for a self-avoiding polymer).[2] This exponent is shown for comparison (dashed line labeled "Zimm model" in the graph). We calculate an experimental exponent $\nu = (1 + d)/(1 + 3d) = 0.58 \pm 0.01$. From the power law fit, we also obtain the average Zimm diffusion coefficient D_{Zimm} of the wormlike micelle of $8.3(1) \times 10^{-12}$ m^2 s^{-1}.

For free diffusion, D is independent of Δ. For bounded diffusion, the apparent diffusion coefficient is smaller than the true diffusion coefficient at long times, when molecules start to feel the effects of the boundaries. The signal attenuation function S(q), which is related to the diffusion coefficient D *via* eqn (2), is modified due to the effect of boundaries. We utilize a simple restricted diffusion model for surfactant diffusion in a one

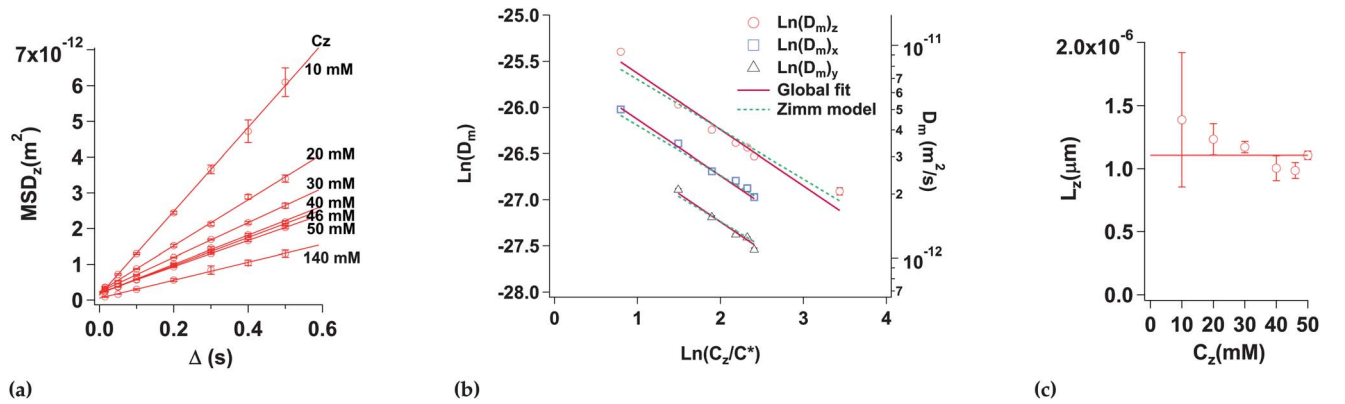

Fig. 5 (a) Z-axis mean square displacement MSD_z *versus* diffusion time Δ. (b) Anisotropic micelle self-diffusion coefficients ($(D_m)_z$,$(D_m)_x$,$(D_m)_y$), extracted from the slopes of the mean-square displacement MSD curves as a function of TDPS concentration (C_z) for TDPS–SDS–NaCl(0.5 M)–D_2O samples at $T = 298$ K. The intercepts are not zero but are on the 0.5 μm scale. (c) The average z-end-to-end distance L_z of the TDPS–SDS micelle *versus* TDPS concentration C_z, extracted from a fit of the signal attenuations using eqn (5), for TDPS–SDS–NaCl(0.5 M)–D_2O samples at $T = 298$ K. The mean L_z is around 1.1 μm.

dimensional wormlike micelle.[50] We modify this to incorporate a diffusing micelle, resulting in the following signal attenuation equation:[50]

$$\ln[S(q)] = -\left((2\pi q)^2\right)D_m\Delta + \ln\left[\frac{2[1-\cos(2\pi qL_z)]}{(2\pi qL_z)^2} + 4(2\pi qL_z)^2 \times \sum_{n=1}^{N}\exp\left(-\frac{n^2\pi^2 D_s\Delta}{L_z^2}\right)\times\frac{1-(-1)^n\cos(2\pi qL_z)}{\left((2\pi qL_z)^2-(n\pi)^2\right)^2}\right]. \quad (5)$$

Here, D_s is the molecular bulk surfactant self-diffusion, D_m is the micellar self-diffusion, $q = \gamma\delta g/(2\pi)$ and L_z is the average length of the one-dimensional channel.

As the diffusion time increases, a larger fraction of molecules feel the effects of confinement, with the diffusion coefficient not changing much for $\Delta \gtrsim 300$ ms. The z-axis signal attenuation curves for each diffusion time in Fig. 4a were fitted to eqn (5). From this fit (signal attenuation curves and fit not shown), we extract the average end-to-end distance L_z (Fig. 5c) for the wormlike micelle. The infinite sum in eqn (5) is approximated by an upper limit $N = 1000$. D_m was obtained from the slopes of Fig. 5a for each TDPS concentration C_z (values obtained for D_m are shown in Fig. 5b). D_s, the free diffusion of surfactant inside a micellar environment, and L_z are fit parameters. A value of $D_s = 13 \times 10^{-12}$ m^2 s^{-1} provided a good fit for all concentrations. Using the Zimm diffusion coefficient D_{Zimm}, the average time τ_{Zimm} for a micellar chain to diffuse a distance of order of its average end-to-end distance L can be calculated.[2] Using $L_{Zimm} = 1.1(1)$ μm and $D_z = 8.3(1) \times 10^{-12}$ m^2 s^{-1}, we get $\tau_{Zimm} \approx (L_{Zimm})^2/D_{Zimm} \approx 0.15$ s.

Rheology and supramicellar structure

Relaxation modulus experiments were performed for a range of TDPS concentrations in the semidilute regime (10 mM $\leq C_z \leq$ 50 mM). If the relaxation modulus exhibits a single exponential at long times, then the recombination and the scission process is rapid, *i.e.* the micellar chain breaks and recombines many times on a time scale $\tau_b \ll \tau_R$ and the primary relaxation mechanism is reptation.[8]

A stress relaxation dominated by a single exponential relaxation decay is generally consistent with the wormlike character of the self-assembled structures in the solution. If $\tau_R \gg \tau_b$, stress relaxation follows a single exponential in wormlike solutions according to the Cates model. Lopez-Diaz *et al.*[41] note that τ_b/τ_R is at a minimum at $R \approx 0.55$, which is precisely the R value where the mixture perfectly fits the Maxwellian Cole–Cole semicircle. While stress relaxation results for $R \approx 0.55$ mixtures could be fitted to Maxwellian viscoelastic behavior with a single relaxation time for the stress relaxation modulus G(t),[41] those for $R \approx 0.43$ showed deviations from the Maxwellian model.[41] For our $R = 0.45$ samples, all the relaxation functions G(t) (not shown) are better fitted to a bi-exponential than a single exponential.

The elastic modulus G_0 (Fig. 6a), associated with the slower, dominant, relaxation mode, is extracted. Reduced viscoelastic spectra are extracted over the whole range of TDPS concentrations C_z. The inset in Fig. 6a is an example of a Cole–Cole diagram for $C_z = 50$ mM. The upturn in G″ at higher frequencies is an expected outcome of Rouse-like behavior.[51] This elastic modulus (Fig. 6a) scales as C_z^b where the exponent b is given[8] by $3\nu/(3\nu - 1) = 3.0 \pm 0.1$, implying $\nu = 0.50 \pm 0.01$. In addition, the zero-shear-strain viscosity (Fig. 6b) also scales[8] as C_z^s with $s = 1/(3\nu - 1) = 2.4 \pm 0.1$, or $\nu = 0.47 \pm 0.01$. Both these scaling behaviors are in the semidilute regime, and consistent with ($\nu = 1/2$) Rouse-like behavior.

Two polymer-like scalings

In this work, we observed two distinct polymer-like scalings in micellar dynamics in the semi-dilute regime. Diffusometry in the semi-dilute regime is consistent with a scaling exponent $\nu = 0.58 \pm 0.01$ (consistent with the value of 0.588 for Zimm-like behavior in a good solvent). On the other hand, rheological measurements are consistent with a random-walk scaling exponent of $\nu = 0.5$.

These results have a simple interpretation. In the semidilute regime of mixed-surfactants TDPS–SDS, NMR diffusometry

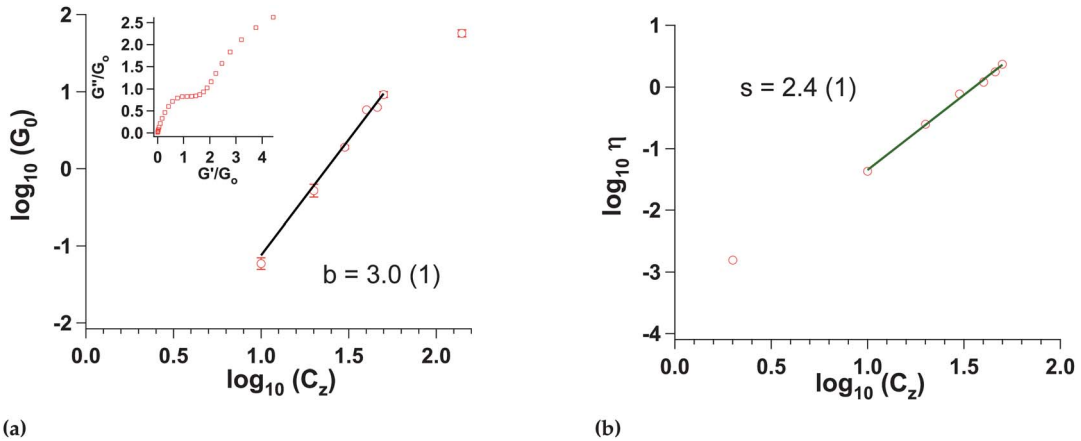

Fig. 6 (a) The elastic modulus G_o *versus* TDPS concentration C_z. Inset: Cole–Cole diagram for $C_z = 50$ mM non-deuterated SDS sample. (b) Zero-shear strain viscosity η *versus* TDPS concentration C_z (on a logarithmic scale) for TDPS–SDS(0.5 M)–D_2O samples. Power law fits in the semi-dilute regime are consistent with the exponent expected for Rouse-like behavior: see text.

provides access to dynamics at shorter lengthscales and times (where hydrodynamic interactions are not screened) and can be described by Zimm dynamics in a good solvent.[2,4] On the other hand, the rheological measurements provide access to dynamics at larger scales at which the hydrodynamic interactions are screened, and Rouse dynamics results. In spite of the fact that the range of the fit is small in order to remain in the semi-dilute regime, the two exponents are distinct (about 8σ apart) and are consistent with classic polymer-like scaling in different hydrodynamic regimes.

Conclusions

In this work, we carried out several complementary NMR experiments, as well as rheology, and these results yield a comprehensive picture of the microscopic structure in a wormlike micellar system. From NMR longitudinal relaxation T_1 measurements (Fig. 2), we estimate the TDPS characteristic overlap concentration $C^* \approx 4.5 \pm 0.4$ mM. This compares reasonably with the value of $\approx$6–7 mM determined using dynamic light scattering.[40] In addition, the temperature dependent ^2H NMR spectra (Fig. 3a) show a single broad deuterium peak that implies the presence of a wide angular distribution in the orientational order, similar to the phenomenon observed in smectics with a high density of quenched disorder.[45]

By measuring the self-diffusion coefficient of the water H_2O molecule in deuterated SDS samples, we were able to obtain the functional dependence of the relative self diffusion coefficient of the water molecules H_2O with respect to the total surfactant volume fraction (Fig. 3c). Often one can assume a single monolayer of surface-associated water.[47] In this system however, there is the equivalent of approximately 3 to 4 layers of surface-associated water. This enhancement of water structure is interesting, and has indeed been reported before in high-salt conditions.[52]

Diffusion time dependence on diffusion coefficients (Fig. 4a), linearity of the mean square displacement MSD *versus* time (but with non-zero offset) (Fig. 5a) and the contrast-matched diffusion experiments all point to a model that includes two ingredients: surfactant restricted diffusion in a cylindrical micelle, and micellar diffusion in water. Therefore, extracting the micellar diffusion from the slopes of the MSD curves (Fig. 5a) and fitting to a simple model with these two ingredients yields an average end-to-end distance of the wormlike micelle in the 1–1.5 μm range and is not strongly concentration-dependent (Fig. 5c), which is not far from the contour length found by Lopez-Diaz *et al.*[41]

Rheology reports on longer timescales and lengthscales than NMR. There appears to be a distinct second relaxation time in the stress relaxation measurements, which is also consistent with oscillatory shear measurements (inset in Fig. 6a) that are not purely Maxwellian. This is consistent with previously reported results[41] which showed deviations from the Maxwellian model at $R = 0.45$.

Finally, two distinct (Zimm and Rouse) polymer-like scalings are observed *via* NMR and rheometry respectively, indicating that the worm-like micelles exhibit classic polymer-like behaviour in different hydrodynamic regimes.

Acknowledgements

We thank the Natural Sciences and Engineering Research Council (NSERC) of Canada for its financial support of this work.

References

1 R. A. L. Jones, *Soft Condensed Matter*, Oxford University Press Inc., New York, 1st edn, 2002.
2 M. Rubinstein and R. H. Colby, *Polymer Physics*, Oxford University Press, New York, 1st edn, 2003.
3 J. F. Douglas and K. F. Freed, *Macromolecules*, 1994, **27**, 6088–6099.
4 P. Ahlrichs, R. Everaers and B. Dunweg, *Phys. Rev. E*, 2001, **64**, 1–4.
5 J.-X. Hou, C. Svaneborg, R. Everaers and G. S. Grest, *Phys. Rev. Lett.*, 2010, **105**, 068301.
6 C. A. Dreiss, *Soft Matter*, 2007, **3**, 956–970.
7 J.-F. Berret, Rheology of wormlike micelles: equilibrium properties and shear banding transitions, in *Molecular Gels: Materials with Self-Assembled Fibrillar Networks*, ed. R. G. Weiss and P. Terech, Springer, The Netherlands, 1st edn, 2006.
8 M. E. Cates and S. J. Candau, *J. Phys.: Condens. Matter*, 1990, **2**, 6869–6892.
9 J. Yang, *Curr. Opin. Colloid Interface Sci.*, 2002, **7**, 267–281.
10 L. M. Walker, *Curr. Opin. Colloid Interface Sci.*, 2001, **6**, 451–456.

11 M. E. Cates, *J. Phys.*, 1988, **49**, 1593–1600.
12 M. E. Cates, *Macromolecules*, 1987, **20**, 2289–2296.
13 M. E. Cates and S. M. Fielding, *Adv. Phys.*, 2006, **55**, 799–879.
14 J. T. Padding, E. S. Boek and W. J. Briels, *J. Chem. Phys.*, 2008, **129**, 074903.
15 J. T. Padding, W. J. Briels, M. R. Stukan and E. S. Boek, *Soft Matter*, 2009, **5**, 4367–4375.
16 D. Lopez-Diaz and R. Castillo, *Soft Matter*, 2011, **7**, 5926.
17 T. Shikata and H. Hirata, *Langmuir*, 1987, **3**, 1081–1086.
18 R. Messager, A. Ott, D. Chatenay, W. Urbach and D. Langevin, *Phys. Rev. Lett.*, 1988, **60**, 1410–1413.
19 S. Candau and R. Oda, *Colloids Surf., A*, 2001, **183–185**, 5–14.
20 R. D. Koehler, S. R. Raghavan and E. W. Kaler, *J. Phys. Chem. B*, 2000, **104**, 11035–11044.
21 P. Fischer, H. Rehage and B. Gruning, *J. Phys. Chem. B*, 2002, **106**, 11041–11046.
22 H. Rehage and H. Hoffmann, *J. Phys. Chem.*, 1988, **92**, 4712–4719.
23 E. Cappelaere, J. F. Berret, J. P. Decruppe, R. Cressely and P. Lindner, *Phys. Rev. E.*, 1997, **56**, 1869–1978.
24 S. J. Candau, E. Hirsch, R. Zana and M. Delsanti, *Langmuir*, 1989, **183–185**, 1225–1229.
25 Z. Lin, J. J. Cai, L. E. Scriven and H. T. Davis, *J. Phys. Chem.*, 1997, **98**, 5984–5993.
26 K. R. Francisco, M. A. da Silva, E. Sabadini, G. Karlsson and C. A. Dreiss, *J. Colloid Interface Sci.*, 2010, **345**, 351–359.
27 T. Shikata, H. Hirata, E. Takatori and K. Osaki, *J. Non-Newtonian Fluid Mech.*, 1988, **28**, 171–182.
28 P. Schurtenberger, R. Scartazzini, L. J. Magid, M. E. Leser and P. L. Luis, *J. Phys. Chem.*, 1990, **94**, 3695–3701.
29 U. Olsson, J. Borjesson, R. Angelico, A. Ceglieb and G. Palazzo, *Soft Matter*, 2010, **6**, 1769–1777.
30 T. S. Davies, Aimee, M. Ketner and S. R. Raghavan, *J. Am. Chem. Soc.*, 2006, **56**, 6669–6675.
31 S. Amin, T. W. Kermis, R. M. van Zanten, S. J. Dees and J. H. van Zanten, *Langmuir*, 2001, **17**, 8055–8061.
32 F. Quirion, *J. Phys. Chem.*, 1986, **90**, 5435–5441.
33 E. Sarmiento-Gomez, D. Lopez-Diaz and R. Castillo, *J. Phys. Chem. B*, 2010, **114**, 12193–12202.
34 P. Schurtenberger and C. Cavaco, *Langmuir*, 1994, **10**, 100–108.
35 P. Schurtenberger, G. Jerke and C. Cavaco, *Langmuir*, 1996, **12**, 2433–2440.
36 S. Forster, M. Konrad and P. Lindner, *Phys. Rev. Lett.*, 2005, **94**, 017803.
37 R. Angelico, G. Palazzo, G. Colafemmina, P. A. Cirkel, M. Giustini and A. Ceglie, *J. Phys. Chem. B*, 1998, **102**, 2883–2889.
38 S. Barhoum and A. Yethiraj, *J. Chem. Phys.*, 2010, **132**, 024909.
39 W. S. Price, F. Tsuchiya and Y. Arata, *J. Am. Chem. Soc.*, 1999, **121**, 11503–11512.
40 D. Lopez-Diaz, E. Sarmiento-Gomez, C. Garza and R. Castillo, *J. Colloid Interface Sci.*, 2010, **348**, 152–158.
41 D. Lopez-Diaz and R. Castillo, *J. Phys. Chem. B*, 2010, **114**, 8917–8925.
42 J. Keeler, *Understanding NMR Spectroscopy*, Wiley, Chichester, USA, 1st edn, 2005.
43 W. S. Price, *Concepts Magn. Reson.*, 1997, **9**, 299–336.
44 W. S. Price, *Concepts Magn. Reson.*, 1998, **10**, 197–237.
45 H. Zeng, B. Zalar, G. Iannacchione and D. Finotello, Effects of quenched disorder on the orientational order of the octylcyanobiphenyl liquid crystal, in *Nuclear Magnetic Resonance Spectroscopy of Liquid Crystals*, ed. Roland Y. Dong, World Scientific Publishing Co. Pte. Ltd., USA, 1st edn, 2009.
46 M. H. Levitt, *Spin Dynamics*, John Wiley, Chichester, 2nd edn, 2008.
47 A. Yethiraj, D. Capitani, N. E. Burlinson and E. E. Burnell, *Langmuir*, 2005, **21**, 3311–3321.
48 R. Angelico, U. Olsson, G. Palazzo and A. Ceglie, *Phys. Rev. Lett.*, 1998, **81**, 2823–2826.
49 A. Das, S. Jayanthi, H. S. M. V. Deepak, K. V. Ramanathan, A. Kumar, C. Dasgupta and A. K. Sood, *ACSNANO*, 2010, **4**, 1687–1695.
50 P. T. Callaghan, *Principles of Nuclear Magnetic Resonance Microscopy*, Clarendon Press, Oxford, New York, 1st edn, 1991.
51 P. Fischer and H. Rehage, *Langmuir*, 1997, **13**, 7012–7020.
52 R. Leberman and A. K. Soper, *Nature*, 1995, **378**, 364–366.

Addition and correction

Note from RSC Publishing

This article was originally published with incorrect page numbers. This is the corrected, final version.

The Royal Society of Chemistry apologises for these errors and any consequent inconvenience to authors and readers.